ITO-free large-area organic light-emitting diodes with an integrated metal grid

Seungkeun Choi, Sung-Jin Kim, Canek Fuentes-Hernandez, and Bernard Kippelen*

School of Electrical and Computer Engineering and Center for Organic Photonics and Electronics, Georgia Institute of Technology, 777 Atlantic Drive, Atlanta, Georgia 30332, USA
**kippelen@gatech.edu*

Abstract: We report on ITO-free large-area organic light-emitting diodes (OLEDs) fabricated on glass substrates comprising α-NPD as a hole transport layer (HTL) and coevaporated CBP:$Ir(ppy)_3$ as the emission layer. Indium-tin-oxide (ITO) was replaced with a conductive polymer electrode and an electroplated thick metal grid was used to improve the homogeneity of the potential distribution over the transparent polymer electrode. An electrical model of a metal grid integrated OLED shows the benefits of the use of metal grids in terms of improving the uniformity of the light emitted as the area of the OLED increases as well as the conductivity of the transparent electrode decreases. By integrating metal grids with polymer electrodes, the luminance increases more than 24% at 6 V and 45% at 7 V compared to the polymer electrode devices without a metal grid. This implies that a lower voltage can be applied to achieve the same luminance, hence lowering the power consumption. Furthermore, metal grid integrated OLEDs exhibited less variation in light emission compared to devices without a metal grid.

OCIS codes: (250.3680) Light-emitting polymers; (160.0160) Optoelectronics; (310.6845) Thin film devices and applications; (310.7005) Transparent conductive coatings; (260.3800) Luminescence

References and links

1. B. Geffroy, P. le Roy, and C. Prat, "Organic light-emitting diode (OLED) technology: materials, devices and display technologies," Polym. Int. **55**(6), 572–582 (2006).
2. K. T. Kamtekar, A. P. Monkman, and M. R. Bryce, "Recent advances in white organic light-emitting materials and devices (WOLEDs)," Adv. Mater. (Deerfield Beach Fla.) **22**(5), 572–582 (2010).
3. A. Haldi, A. Kimyonok, B. Domercq, L. E. Hayden, S. C. Jones, S. R. Marder, M. Weck, and B. Kippelen, "Optimization of orange-emitting electrophosphorescent copolymers for organic light-emitting diodes," Adv. Funct. Mater. **18**(19), 3056–3062 (2008).
4. K. Saxena, V. K. Jain, and D. S. Mehta, "A review on the light extraction techniques in organic electroluminescent devices," Opt. Mater. **32**(1), 221–233 (2009).
5. R. Bathelt, D. Buchhauser, C. Gärditz, R. Paetzold, and P. Wellmann, "Light extraction from OLEDs for lighting applications through light scattering," Org. Electron. **8**(4), 293–299 (2007).
6. T.-W. Koh, J.-M. Choi, S. Lee, and S. Yoo, "Optical outcoupling enhancement in organic light-emitting diodes: highly conductive polymer as a low-index layer on microstructured ITO electrodes," Adv. Mater. (Deerfield Beach Fla.) **22**(16), 1849–1853 (2010).
7. Y. Sun and S. R. Forrest, "Enhanced light out-coupling of organic light-emitting devices using embedded low-index grids," Nat. Photonics **2**(8), 483–487 (2008).
8. S. Choi, W. J. Potscavage, and B. Kippelen, "ITO-free large-area organic solar cells," Opt. Express **18**(S3 Suppl 3), A458–A466 (2010).
9. R. Paetzold, K. Heuser, D. Henseler, S. Roeger, G. Wittmann, and A. Winnacker, "Performance of flexible polymeric light-emitting diodes under bending conditions," Appl. Phys. Lett. **82**(19), 3342–3344 (2003).
10. J. R. Sheats and D. B. Roitman, "Failure modes in polymer-based light-emitting diodes," Synth. Met. **95**(2), 79–85 (1998).
11. K. Fehse, K. Walzer, K. Leo, W. Lövenich, and A. Elschner, "Highly conductive polymer anodes as replacements for inorganic materials in high-efficiency organic light-emitting diodes," Adv. Mater. (Deerfield Beach Fla.) **19**(3), 441–444 (2007).
12. D. Krautz, S. Cheylan, D. S. Ghosh, and V. Pruneri, "Nickel as an alternative semitransparent anode to indium tin oxide for polymer LED applications," Nanotechnology **20**(27), 275204 (2009).

#143145 - $15.00 USD Received 23 Feb 2011; revised 15 Apr 2011; accepted 21 Apr 2011; published 6 Jun 2011

13. H. Chang, G. Wang, A. Yang, X. Tao, X. Liu, Y. Shen, and Z. Zheng, "A transparent, flexible, low-temperature, and solution-processible graphene composite electrode," Adv. Funct. Mater. **20**(17), 2893–2902 (2010).
14. K. Neyts, M. Marescaux, A. U. Nieto, A. Elschner, W. Lovenich, K. Fehse, Q. Huang, K. Walzer, and K. Leo, "Inhomogeneous luminance in organic light emitting diodes related to electrode resistivity," J. Appl. Phys. **100**(11), 114513 (2006).
15. K. Neyts, A. Real, M. Marescaux, S. Mladenovski, and J. Beeckman, "Conductor grid optimization for luminance loss reduction in organic light emitting diodes," J. Appl. Phys. **103**(9), 093113 (2008).
16. J. Park, J. Lee, D. Shin, and S. Park, "Luminance uniformity of large-area OLEDs with an auxiliary metal electrode," J. Disp. Technol. **5**(8), 306–311 (2009).
17. S. Harkema, S. Mennema, M. Barink, H. Rooms, J. S. Wilson, T. van Mol, and D. Bollen, "Large area ITO-free flexible white OLEDs with Orgacon PEDOT:PSS and printed metal shunting lines," in *Organic Light Emitting Materials and Devices XIII*, (SPIE, 2009), 74150T–74158.
18. M. G. Kang and L. J. Guo, "Nanoimprinted semitransparent metal electrodes and their application in organic light-emitting diodes," Adv. Mater. (Deerfield Beach Fla.) **19**(10), 1391–1396 (2007).
19. S. Choi, W. J. Potscavage, Jr., and B. Kippelen, "Area-scaling of organic solar cells," J. Appl. Phys. **106**(5), 054507 (2009).
20. S. Choi, W. J. Potscavage, Jr., and B. Kippelen, "Area-scaling of organic solar cells and integrated modules," in *Organic Materials and Devices for Sustainable Energy Systems*, J. Xue, ed. (Mat. Res. Soc. Symp. Proc., Boston, MA, USA, 2009), p. S06.
21. A. Sharma, P. J. Hotchkiss, S. R. Marder, and B. Kippelen, "Tailoring the work function of indium tin oxide electrodes in electrophosphorescent organic light-emitting diodes," J. Appl. Phys. **105**(8), 084507 (2009).
22. M.-H. Ho, M.-T. Hsieh, K.-H. Lin, T.-M. Chen, J.-F. Chen, and C. H. Chen, "Study of efficient and stable organic light-emitting diodes with 2-methyl-9,10-di(2-naphthyl)anthracene as hole-transport material by admittance spectroscopy," Appl. Phys. Lett. **94**(2), 023306 (2009).

1. Introduction

Organic light-emitting diodes (OLEDs) have been extensively studied in recent years due to their potential for the development of low-cost, bright and light-weight display panels, and for lighting applications with highly flexible form factors [1]. Significant efforts have been focused on improving the power efficiency through the synthesis of new light-emitting molecules and polymers [2,3], and through novel light extracting architectures [4–7]. Although indium-tin-oxide (ITO) is the most widely used transparent electrode for both OLEDs and organic photovoltaics (OPVs), there is a great interest to find low-cost alternatives because its use in devices such as LCD panels and touch-screen displays has lead to an increased demand and to strong price volatility due to supply concerns [8]. Furthermore, ITO has poor mechanical properties when deposited on flexible substrates, making it susceptible to cracks when the substrates are bent [9]. In addition, there have been concerns of migration of indium from ITO into the emission layers during OLED operation, thereby decreasing their lifetime [10]. Hence, developing an OLED architecture in which ITO is replaced with a transparent, low-cost, indium-free, and crack-tolerant electrode is of great interest. Furthermore, since demands for large-area OLEDs for display and lighting applications are increasing, uniform light emission and low-power consumption also must be considered.

Transparent conductive electrodes used in prior studies to replace ITO in small-area OLEDs devices include the highly conductive polymer poly (3,4–ethylenedioxythiophene): poly(styrenesulfonate) (PEDOT:PSS) [11], semitransparent metal electrodes [12] as well as graphene composite electrodes [13]. While all these electrodes can achieve a performance comparable to that of ITO in terms of transmittance and conductance, they generally do not provide solutions to the fabrication of large-area OLEDs where a large potential gradient is expected as the area of the device increases, hence degrading the uniformity of the light emitted. The uniformity of the light emitted can be improved by utilizing a metal grid [14,15], which will also contribute to reduce the power consumed at a desired luminance. Although there have been several approaches where thin metal grids, typically thinner than 100 nm, are combined with ITO or PEDOT:PSS [16–18], in large-area OLEDs, the inhomogeneous potential distribution and high power consumption generated by such thin metal grids themselves cannot be ignored, especially in lighting applications that require high luminance.

Recently, we reported on the improvement of performance of large-area organic solar cells and modules by integrating thick metal grids directly with ITO [19,20], and also with a highly conductive polymer electrode [8]. Because of the electroplating approach, thick grids were

#143145 - $15.00 USD Received 23 Feb 2011; revised 15 Apr 2011; accepted 21 Apr 2011; published 6 Jun 2011

realized, with a thickness typically more than a few micro meters, enabling a large current to flow with significantly less potential drop across the large-area device.

In this work, we present ITO-free large-area OLEDs fabricated on glass substrates comprised of α-NPD, as a hole transport layer (HTL), and coevaporated CBP:Ir(ppy)$_3$ [21], as the emission layer. A highly conductive PEDOT:PSS formulation (Clevios PH 1000, H. C. Starck) was selected as a hole-injecting transparent electrode and was combined with a thick metal grid structure designed to form good electrical contact with the polymer electrode. The active area of the devices was 7.3 cm^2. The performance of OLEDs with the conducting polymer was first compared with that of reference devices using ITO as the transparent electrode. Then, metal grids were integrated in both, an ITO-free OLED and a reference device, and their performance was compared with OLEDs without a metal grid.

2. Experiment

The devices under study were comprised of a highly conductive PEDOT:PSS layer (H.C. Stark, Clevios PH 1000, 140 nm) followed by a thin layer of PEDOT:PSS (Clevios AI 4083, 40 nm) as a transparent anode. Figure 1 shows the general structure of the ITO-free large area OLEDs fabricated on glass substrates for this study. OLEDs with an ITO electrode, instead of a polymer electrode, were also fabricated as a reference and their performance compared with those of the ITO-free OLEDs. Metal grids were integrated with a PEDOT:PSS and with an ITO electrode in order to improve the uniformity of light emission.

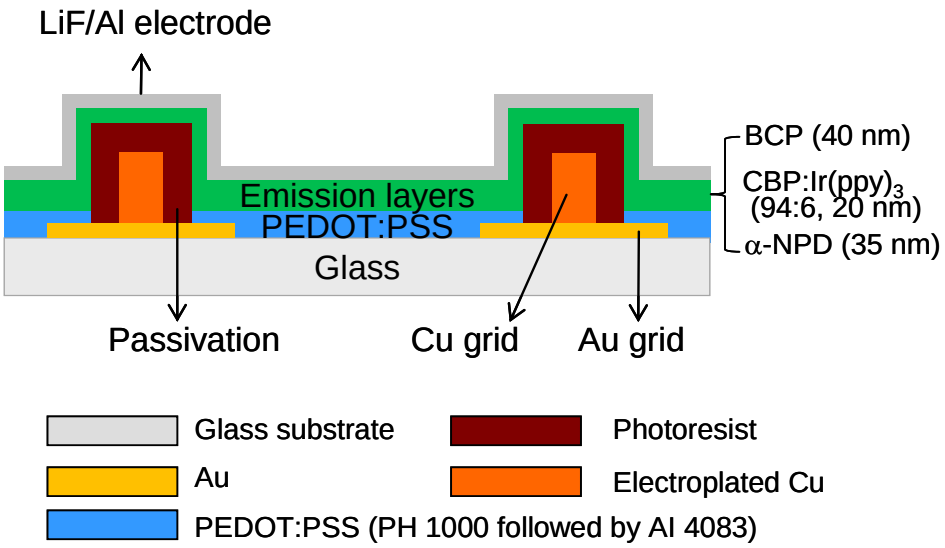

Fig. 1. Device geometry of ITO-free large-area OLED with a grid. The grid was composed of two metal layers: sputtered Au (100 nm) and electroplated Cu (5 μm). The thin Au grid connects the PEDOT:PSS electrode to the thick Cu grid. For a device with an ITO electrode, the metal grid only consisted of electroplated copper, which made direct contact with the underlying ITO.

Substrate preparation: ITO-coated glass was purchased from Colorado Concept Coatings LLC (sheet resistance of 11.1 Ω/sq., 136 nm thick) and cut into 1.5 inch by 1.5 inch squares. For the devices with an ITO electrode, the ITO was patterned using chemical wet etching ($HCl:H_2O_2:H_2O$ = 3:1:4) to define the active area. For the ITO-free devices, the ITO was completely removed by using the same chemical etchant. Then, the substrates were cleaned in sequential ultrasonic baths of soap, acetone, and isopropanol for 60 minutes each.

Metal grid fabrication: For ITO-free devices, a metal grid was fabricated on top of a glass substrate from which the ITO-coating had been completely removed. 10 nm of Cr and 100 nm of Au were sequentially sputtered (Unifilm Technology PVD-300) on the glass and patterned

#143145 - $15.00 USD Received 23 Feb 2011; revised 15 Apr 2011; accepted 21 Apr 2011; published 6 Jun 2011

using photolithography to create finger and busbar electrodes (Fig. 2(a)). Next, seed layers of 10 nm of chrome and 150 nm of copper were deposited all over the surface using a filament evaporator (Kurt J. Lesker PVD-75 Filament Evaporator). Electroplating mold structures were created on top of the seed layers with a photoresist (Shipley SPR220) (Fig. 2(b)). A copper plating solution was prepared by mixing 250 mg of $CuSO_4$-$5H_2O$ and 25 ml of H_2SO_4 in 1 liter of deionized water. 5 µm-thick electrodes of copper were electroplated by applying a dc current with a current density of 15 mA/cm^2 (Fig. 2(c)). The mold structures were removed using a photoresist remover (Shipley Microposit Remover 1165 at 80 °C for 10 minutes). The electroplated grids were completely insulated with a photoresist (Futurex NR9-8000P) to prevent any electrical shorts between the thick metal grid and the LiF/Al top electrode (Fig. 2(d)). Finally, the chromium and copper seed layers were removed by wet chemical etching, and part of the Au grid electrode was opened to make contact with the polymer electrode that was spin-coated on top. The width of the Cu grid finger electrodes was 25 µm with a finger spacing of 2.48 mm. The width of the busbar was 300 µm. The patterned Au electrodes were 80 µm wider than the Cu grid electrodes in order to allow for good electrical contact with the PEDOT:PSS layer. Without the Au layer, the passivation of the Cu grid that is necessary to prevent shorts with the top Al electrode, makes it difficult to have good electrical contact between the Cu grid and the PEDOT:PSS layer. The opaque area introduced by the metal grid is 5.5% of the total active area (7.3 cm^2 for OLEDs with polymer electrode). In devices where the metal grid was fabricated on top of an ITO electrode, the underlying patterned Au pads were not necessary, resulting in a reduction of the total active area by only 2.2%.

Organic semiconductor deposition: For the ITO-free devices, a polymer electrode was spin-coated on top of the grid from a solution of Clevios PH 1000 PEDOT:PSS (H. C. Starck) mixed with 5%, by volume, of dimethyl sulfoxide (DMSO) to increase conductivity and annealed for 20 min. on a hotplate at 140 °C in air. The polymer electrode was patterned using plasma reactive ion etching (RIE) (Plasma Therm RIE) to create an active area of 7.3 cm^2. To smooth the surface, another layer of PEDOT:PSS (Clevios Al 4083) was spin-coated and annealed on a hotplate at 140°C for 10 min. in air (Fig. 2(e)). For the device with ITO, the PEDOT:PSS (Clevios AI 4083) was spin-coated on top of ITO and annealed for 20 min. on a hotplate at 140°C in air. Then, the devices were transferred into a vacuum thermal evaporator (Spectros, Kurt J. Lesker) which is connected to a nitrogen-filled glovebox. For the hole-transport layer, 35 nm of benzyl 3,3′,3”-(2'-(3-(9H-carbazol-9-yl)phenyl)-9,9'-spirobi[fluorene]-2,7,7'-triyl)tribenzoate (α-NPD) were deposited at a rate of 0.4 Å/s. For the emitting layer, $Ir(ppy)_3$ was coevaporated at a concentration of 6 wt. % into a 20-nm-thick film of 4,4’-di(carbazol-9-yl)-biphenyl (CBP). For the hole-blocking and electron transport layer, BCP was deposited at rates of 0.4 Å/s, respectively. Finally, 2.5 nm of lithium fluoride (LiF) as an electron-injection layer and a 200 nm-thick aluminum cathode were deposited at rates of 0.1 Å/s and 2 Å/s, respectively. The testing was done right after the deposition of the metal cathode in an inert atmosphere, without exposing the devices to air.

#143145 - $15.00 USD Received 23 Feb 2011; revised 15 Apr 2011; accepted 21 Apr 2011; published 6 Jun 2011

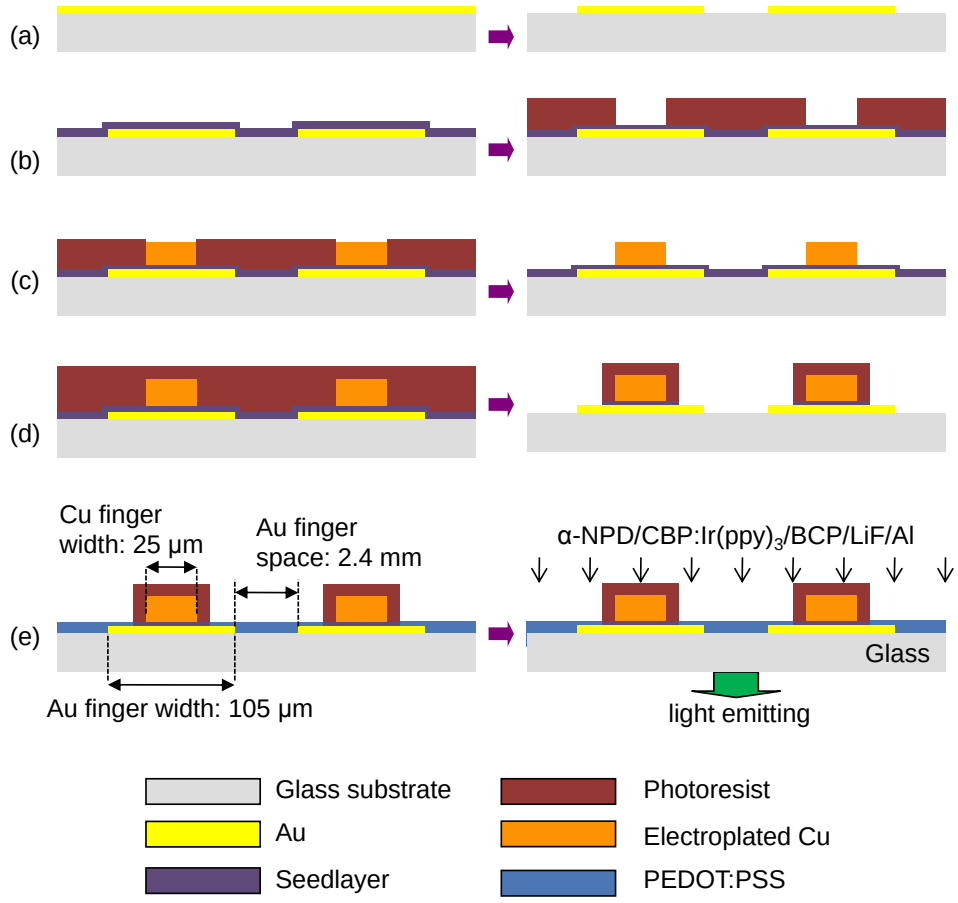

Fig. 2. Fabrication sequences for ITO-free large-area OLED with a grid: (a) Au deposition and grid patterning; (b) seedlayers deposition and mold structure creation; (c) copper grid electroplating and mold structure removal; (d) copper grid passivation and seedlayer removal; (e) PEDOT:PSS (Clevios PH1000 followed by AI 4083) spin-coating, and organic layers and LiF/Al electrode deposition.

3. Metal grid modeling

An electrical model is presented here to describe how the sheet resistance of a transparent electrode affects the uniformity of the emitted light in an OLED and the effects of including a metal grid into its structure. The metal grids consisted of finger electrodes branching from a busbar to provide low resistance paths for the supplied current. We considered three thin film layers and two finger electrodes in order to model a metal grid integrated OLED: a transparent bottom electrode, an emission layer, a top electrode (usually highly conductive metal electrode such as Al), and two thick finger electrodes separated by a distance s on both edges as shown in Fig. 3. The voltage drop is only considered at the bottom electrode (along the x-axis in Fig. 3). The voltage drops across the top electrode and the metal grid are ignored because their conductivity is at least two orders of magnitude higher than the bottom electrode. The current density flowing in the emission layer, j_Z (perpendicular to the substrate), and at the bottom electrode, j_{bot} (parallel to the substrate), are assumed to be only a function of x. Here, for simplicity it is also assumed that the luminous efficiency η (cd/A) is constant, such that the luminance (L) can be considered proportional to the current density j_Z ($L = \eta \times j_Z$) [14].

#143145 - $15.00 USD Received 23 Feb 2011; revised 15 Apr 2011; accepted 21 Apr 2011; published 6 Jun 2011

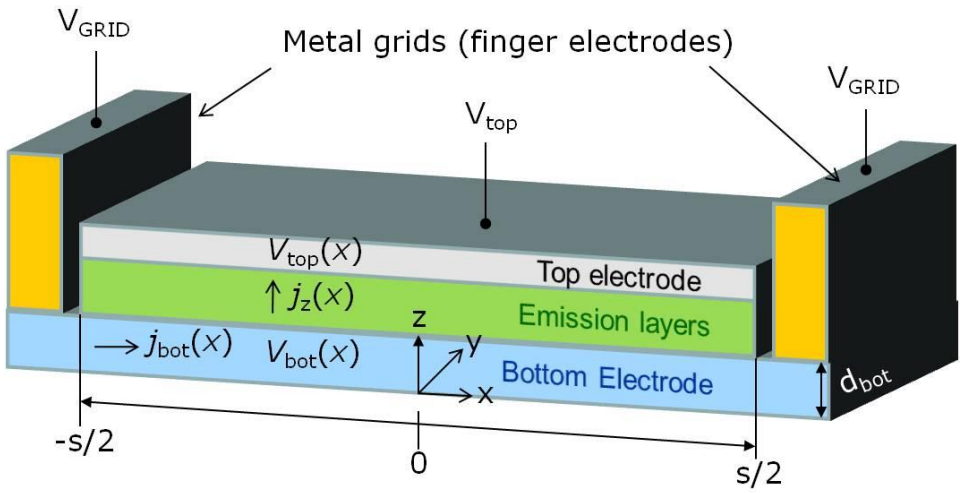

Fig. 3. Geometry of the metal-grid integrated large-area OLED used in the electrical model.

The current density in the bottom electrode along x, j_{bot}, can be expressed as

$$\vec{j}_{bot}(x) = -\sigma_{bot} \cdot \vec{\nabla} V_{bot}(x) \tag{1}$$

Where σ_{bot} is the electrical conductivity of the bottom layer and V_{bot} is the electrostatic potential.

By assuming steady-state conditions and conservation of the electric charge, j_Z can be expressed using the divergence operator as,

$$j_z(x) = -\vec{\nabla} \cdot (d_{bot}\, \vec{j}_{bot}(x)) \tag{2}$$

where the negative sign implies an outgoing current density. Combining Eq. (1) and (2) leads to the following differential equation,

$$\nabla^2 \cdot V_{bot}(x) = \frac{1}{\sigma_{bot} d_{bot}} j_z(x) \tag{3}$$

In order to solve this equation, we need one more equation which relates j_Z with V_{bot}. Since the voltage differences introduced by the bottom electrode are rather small we can approximate the voltage characteristic around the average operating voltage as linear:

$$j_z(x) = j_z(x=0) + a(V_{bot}(x) - V_{top}(x)) \tag{4}$$

which states that the j_Z is proportional to the voltage difference between the top and bottom electrodes. A proportionality factor, a [1/(Ωcm^2)], represents how conductive the emission layer is in the forward biased region. Assuming a perfectly conducting top electrode, *i.e.*, $V_{top}(x) = 0$, Eq. (4) becomes,

$$V_{bot}(x) = (1/a)(j_z(x) - j_z(0)) \tag{5}$$

Removing $V_{bot}(x)$ in Eq. (3) using Eq. (5) yields,

$$\nabla^2 \cdot j_z(x) - a \cdot R_{\Omega/sq} \cdot j_z(x) = 0 \tag{6}$$

where $R_{\Omega/sq}$ is the sheet resistance of the bottom electrode (units of Ω/sq.) and is given by Eq. (7),

#143145 - $15.00 USD Received 23 Feb 2011; revised 15 Apr 2011; accepted 21 Apr 2011; published 6 Jun 2011

$$R_{\Omega/sq} = \frac{1}{\sigma_{bot} d_{bot}} \tag{7}$$

Since $j_Z(x)$ is symmetric with respect to $x = 0$, the solution of Eq. (6) is given by,

$$j_z(x) = \frac{j_z(0)}{2}\left(e^{(\sqrt{aR_{\Omega/sq}})x} + e^{-(\sqrt{aR_{\Omega/sq}})x}\right) \tag{8}$$

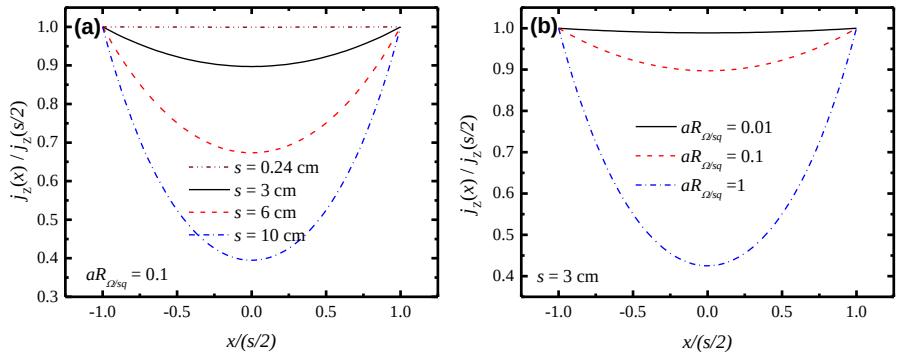

Fig. 4. Normalized current density, $j_Z(x)$ divided by $j_Z(s/2)$, as a function of normalized position coordinate ($x/(s/2)$) a) for different grid spacings and b) for different values of $a \times R_{\Omega/sq}$. Note that $a \times R_{\Omega/sq} = 0.1$ and 1.0 correspond to OLEDs fabricated with ITO only or with a polymer electrode, respectively.

Figure 4(a) shows the normalized current density, $j_Z(x)/j_Z(s/2)$, as a function of the normalized position coordinate $x/(s/2)$, obtained from Eq. (8) for three different grid spaces, s = 3, 6, and 10 cm with $a \times R_{\Omega/sq} = 0.1$. Note that under this normalization of the x coordinate, the grid electrodes are always located at −1 and 1. Figure 4(a) clearly shows that as the distance between finger electrodes increases, the value of $j_Z(x)/j_Z(s/2)$ in the inter-grid space decreases. This means that the current density at a given location decreases as its distance from the finger electrode increases. For example, considering $a \times R_{\Omega/sq} = 0.1$, we found that when the finger electrodes are 3 cm apart, s = 3 cm, the current density at the center of the grid electrodes is 89.7% of that found at the grid electrodes. However, this drop increases to 67.3% and 39.5% for grid spacing's of 6 cm and 10 cm, respectively. This implies that to obtain similar values of L, a much larger voltage will be required in OLEDs with larger grid spacings. On the other hand, according to Eq. (8), the decrease in $j_Z(x)/j_Z(s/2)$ also depends on the sheet resistance. Figure 4(b) shows the normalized current density, $j_Z(x)/j_Z(s/2)$, as a function of the normalized position coordinate $x/(s/2)$ for three different values of $a \times R_{\Omega/sq}$ = 0.01, 0.1, and 1 for s = 3 cm. This grid spacing corresponds to the device length of OLEDs without a grid we have fabricated for this work and will be discussed in details later. As clearly shown in Fig. 4(b), as $R_{\Omega/sq}$, increases at a given proportionality factor, a, the value of $j_Z(x)/j_Z(s/2)$ in the inter-grid space decreases dramatically. This shows that transparent electrodes with a low sheet resistance are necessary to yield a uniform light emission. Furthermore, since the proportionality factor, a, represents the conductivity of the emissive layer, a more uniform light emission can also be expected for smaller values of a; this is, for emissive layers with higher resistance. Hence, for OLEDs with large values of $a \times R_{\Omega/sq}$, the use of a metal grid can have a strong impact in improving the uniformity of its emitted light and in reducing its operating voltage. However, there is a trade-off as the amount of light blocked by the metal grids is increased as the distance between finger electrodes is decreased.

#143145 - $15.00 USD Received 23 Feb 2011; revised 15 Apr 2011; accepted 21 Apr 2011; published 6 Jun 2011

4. Performance of ITO-free large-area OLED with an integrated metal grid

The sheet resistance of 140 nm-thick layers of PEDOT:PSS was measured using the transmission line method and yielded a value of 101 ± 4 Ω/sq, to be compared with 11.1 ± 0.1 Ω/sq for ITO (136 nm). Reference devices were also fabricated on ITO with- and without- a grid. Figure 5(a) and 5(b) shows the current density - voltage (*J-V*) curves of the ITO-free devices with- and without- a grid as well as reference devices with- and without- a grid. Figure 5(c) shows the luminance (*L*) and external quantum efficiency (EQE) as a function of applied voltage for these devices. All devices have a similar turn on voltage at around 3.4 V. However, devices with a grid exhibit higher luminance at a given voltage compared to devices without a grid and this improvement becomes significant as an applied voltage continues to increase. This is because the value of the proportionality factor, *a*, is higher at higher applied voltage, thereby exhibiting higher value of $j_z(x)/j_z(s/2)$ compared to the values found at a lower voltage level, as shown in Fig. 4(b). This means that larger improvements on the uniformity of the current distribution can be obtained using the metal grids, as shown in Fig. 4(a). For example, in devices with an ITO electrode, the luminance increases more than 33% (from 1184 to 1581 cd/m^2) at 6 V and 78% (from 2442 to 4347 cd/m^2) at 7 V in OLEDs that use the metal grids compared with those that do not use metal grids (Fig. 5(c)). The same trends are observed with the ITO-free devices; the luminance increases more than 24% (from 1048 to 1308 cd/m^2) at 6V and 45% (from 2278 to 3321 cd/m^2) at 7V in OLEDs with a metal grid compared with devices without it. This implies that a lower voltage can be applied to achieve the same luminance by integrating the metal grids with the transparent electrodes. This improvement can be attributed to the thick metal grids which transfer more current into the emission layer at a given voltage. However, as expected from the otherwise identical composition, the use of metal grids does not make any significant difference in the EQE of the OLEDs, as is shown in Table 1. For example, the efficiencies measured at 100 and 1000 cd/m^2 for the devices with an ITO electrode were 15.7% and 12.4% when a metal grid was not used, and were 16.0% and 12.7% with a metal grid. The same trends are found with the ITO-free devices. The efficiencies measured at 100 and 1000 cd/m^2 are summarized in Table 1.

Table 1. Summary of the EQE and Luminous Efficiency (cd/A) at 100 and 1000 cd/m^2 for the Devices with an ITO Electrode and Devices with a Polymer Electrode (PH 1000)

Transparent electrode			100 cd/m^2		1000 cd/m^2	
Device #	Anode (cm^2)	Grid	EQE [%]	Luminous efficiency (cd/A)	EQE [%]	Luminous efficiency (cd/A)
1	ITO (7.2)	without a grid	15.7	53.5	12.4	42.0
2	Polymer (7.3)	without a grid	10.9	37.2	8.6	29.5
3	ITO (7.0)	with a grid	16.0	54.7	12.7	43.6
4	Polymer (7.3)	with a grid	11.3	39.1	8.7	29.8

The ITO-free device without a grid (device # 2) exhibits about 30% and 31% lower EQE at 100 and 1000 cd/m^2, respectively, compared to the device with the ITO electrode (device #1). Similar results were obtained from the ITO-free device with a grid (device #4) which showed about 29% and 31% lower EQE at 100 and 1000 cd/m^2 compared to the device with the ITO electrode (device #3), respectively. In other words, devices with polymer electrodes exhibit lower EQE and luminous efficiency. This can be partly attributed to inferior optical properties of PEDOT:PSS (PH 1000) compared to ITO. For example, it has been shown that the transmittance at a wavelength of 510 nm is 96.3% for ITO (136nm in thickness) and 89.2% for PH 1000 polymer electrode (134nm in thickness) [8]. However, a lower transmittance alone cannot account for the lower efficiency of the devices with polymer electrodes. Instead, these differences could be related to changes in hole injection efficiency at the interface formed by the hole transport layer and the different materials used as electrodes. The results suggest that the PEDOT:PSS electrode could be responsible for a larger hole injection and a

#143145 - $15.00 USD Received 23 Feb 2011; revised 15 Apr 2011; accepted 21 Apr 2011; published 6 Jun 2011

corresponding imbalance between the holes and electrons flowing into the emissive layer. This imbalance reduces the EQEs in OLEDs with the polymer electrodes compared with the better balanced OLEDs with ITO electrodes [22]. This hypothesis seems to be well supported by the larger current densities observed, at a given voltage, in the devices with a polymer electrode compared to those with an ITO electrode (Fig. 5(a) and 5(b)). For example, in devices without a grid, the polymer devices exhibited as much as 15%, 25%, and 37% higher current density compared to devices with ITO at 5 V, 6 V, and 7 V, respectively. For devices with a grid, the polymer devices exhibited as much as 22%, 17%, and 7% higher current density compared to devices with ITO at 5 V, 6 V, and 7 V, respectively.

If we calculate the proportionality factor, a, used in our model, from the current-voltage measurements in our OLEDs without a grid, we obtain values of 8.9×10^{-3} and 10.9×10^{-3} A/V at 5 V for OLEDs with an ITO and a polymer electrode, respectively. For ITO, a sheet resistance of 11.1 Ω/sq yields a value of $a \times R_{\Omega/sq} = 0.1$. In contrast, for the polymer electrode with a sheet resistance of 101 Ω/sq, the value of $a \times R_{\Omega/sq} = 1.1$, which is one order of magnitude larger. Since the device lengths of OLEDs with ITO and polymer electrodes were 2.9 and 3.0 cm, respectively, Fig. 4(b) provides an approximate picture of the differences in the uniformity of the light emitted between OLEDs with the ITO electrode and a polymer electrode when no grid is used. For example, considering $s = 3$ cm, we found that when the ITO electrode was used, $a \times R_{\Omega/sq} = 0.1$, the current density at the center of the OLED is 90% of that found at the edges of the OLED; and drops to 42% for the OLED with the polymer electrode. However, as shown in Fig. 4(a), when we use a metal grid with s = 0.24 cm, the current density at the center of the grid electrodes is calculated to be 99.9% of that found at the grid electrodes for the OLED with an ITO electrode. Although it is not shown in Fig. 4(a), the same trend is observed with the ITO-free device ($a \times R_{\Omega/sq} = 1.1$); the current density at the center of the grid electrodes is 99.3% of that found at the grid electrodes for OLED with a polymer electrode despite its significantly larger $a \times R_{\Omega/sq}$ factor.

Figure 6 shows pictures of ITO-free OLEDs with- and without- metal grids taken at various applied voltages. A Pentax K10D camera and the same exposure settings (ISO 100, 1/30sec, F/2) were used for all pictures without post imaging process except cropping. The white color in the pictures is due to the saturation of the image sensor in the camera. Because of the higher luminance of the device with a grid, the camera sensor saturates at lower voltage compared to the device without a grid. Subsequent more detailed measurements of the uniformity of the emission across the OLED were impaired by the degradation of the devices and appearance of dark spots. Although a quantitative comparison cannot be drawn from these pictures in order to establish a direct comparison with the modeled values, qualitatively it seems clear that, particularly at high voltages, the device without a grid shows a less-uniform light emission between the center and its edges, than the one with the grid. Furthermore, it should be noted that this difference is already evident in devices with a total area (around 7 cm^2) which could be considered small for lighting applications. If OLEDs with a larger area are fabricated without a metal grid, much larger differences in light uniformity and higher operating voltages would be expected compared with an OLED having a metal grid integrated electrode. Hence, it should be noted while the properties of OLEDs without a metal grid are strongly dependent on its area, the properties of the OLEDs with the metal grid integrated electrodes are essentially area independent once the grating spacing is defined. Therefore, the use of metal grid integrated electrodes is expected to open the door to the use of low-cost conductive polymers for flexible, low-cost, large area OLEDs lighting applications.

#143145 - $15.00 USD Received 23 Feb 2011; revised 15 Apr 2011; accepted 21 Apr 2011; published 6 Jun 2011

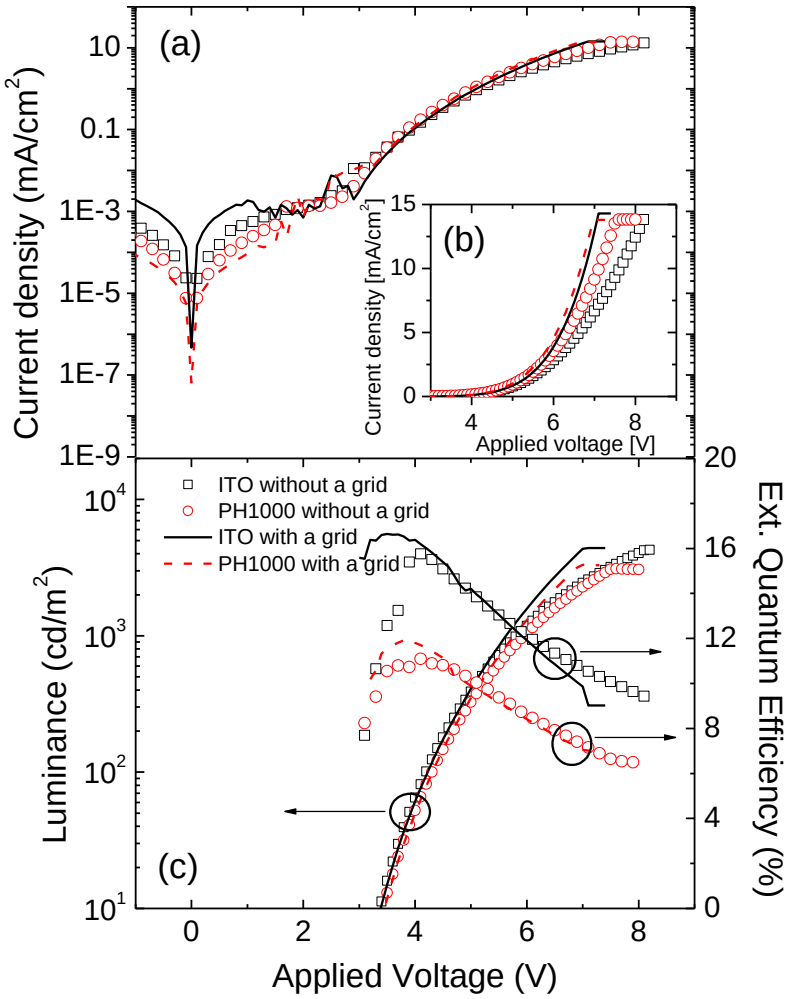

Fig. 5. Experimental *J-V* characteristics in semi-logarithmic scale (a), linear scale (b), and the luminance and EQE (c) of the ITO-free OLEDs and reference devices with ITO.

#143145 - $15.00 USD Received 23 Feb 2011; revised 15 Apr 2011; accepted 21 Apr 2011; published 6 Jun 2011

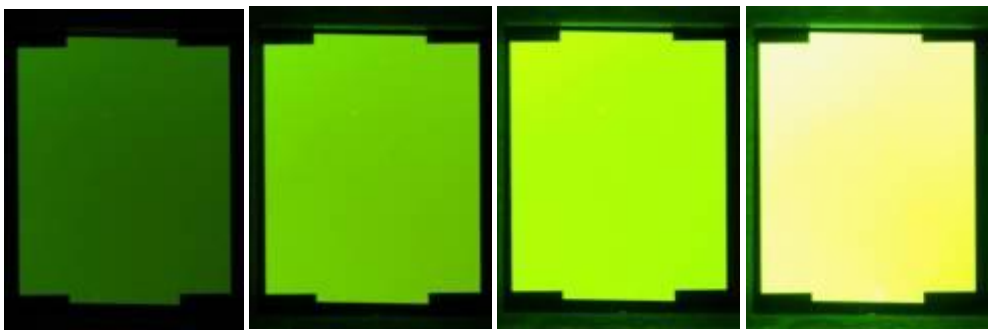

(a) no grid, 3.5 V (b) no grid, 4.0 V (c) no grid, 4.5 V (d) no grid, 5.0 V

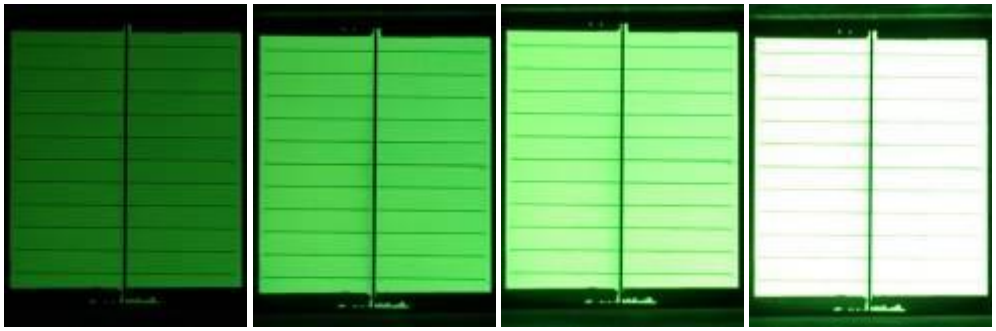

(e) with grid, 3.5 V (f) with grid, 4.0 V (g) with grid, 4.5 V (h) with grid, 5.0 V

Fig. 6. Photographs taken at various applied voltages. (a)–(d): ITO-free large-area OLED without a metal grid, (e)–(h): ITO-free large-area OLED with a grid.

5. Conclusions

In summary, we demonstrated an ITO-free large-area (7.3 cm^2) OLED by integrating metal grids with a highly conductive grade of PEDOT:PSS (Clevios PH 1000, H. C. Starck). An electrical model of the metal grid integrated OLED was presented in order to show how the grid spacing and sheet resistance of the transparent electrode affects the uniformity of the light emitted. For both, the ITO-free devices and the reference devices with an ITO, the use of thick metal grids contributes to achieve a higher luminance at a given voltage, and at the same time, improves the uniformity of the light emitted. Although the devices with a polymer electrode exhibited relatively lower efficiencies compared to the devices with an ITO, we attribute this difference primarily to a poor balance between injected holes and electrons, which could be improved with further device optimization. Because metal grid integrated electrodes relax the stringent requirement for high conductivity transparent electrodes and because they make the properties of the OLEDs independent of its area, we believe that the demonstration of efficient metal-grid integrated OLEDs is a step forward towards the development of low-cost, free-form and efficient large area OLEDs that could be used for lighting applications.

Acknowledgments

This material is based upon work supported in part by the STC Program of the National Science Foundation under Agreement No. DMR-0120967 and by the Office of Naval Research. This work was performed in part at the Microelectronics Research Center at Georgia Institute of Technology, a member of the National Nanotechnology Infrastructure Network, which is supported by NSF (Grant No. ECS- 03-35765).

#143145 - $15.00 USD Received 23 Feb 2011; revised 15 Apr 2011; accepted 21 Apr 2011; published 6 Jun 2011